Engineering Structures 254 (2022) 113774

Contents lists available at ScienceDirect

Engineering Structures

journal homepage: www.elsevier.com/locate/engstruct

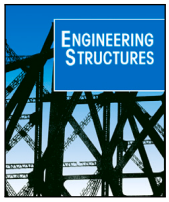

Non-Gaussian turbulence induced buffeting responses of long-span bridges based on state augmentation method

Wei Cui, Lin Zhao *, Yaojun Ge

State Key Lab of Disaster Reduction in Civil Engineering, Tongji University, Shanghai 200092, China
Department of Bridge Engineering, College of Civil Engineering, Tongji University, Shanghai 200092, China
Key Laboratory of Transport Industry of Bridge Wind Resistance Technologies, Tongji University, Shanghai 200092, China

ARTICLE INFO

Keywords:
Long span bridge
Buffeting response
Non-Gaussian turbulence
State augmentation method
Ornstein–Uhlenbeck process

ABSTRACT

Traditionally, the structural turbulence-induced buffeting vibrations is analyzed along the famous Davenport chain through turbulence, wind loads and structural response based on one fundamental assumption: the random processes about the above three subsequent stages should be all Gaussian process. This assumption simplifies the mathematical derivation of turbulence-induced vibration, and were widely used in field of wind engineering for structures. However, several recent studies reveal that turbulence with non-Gaussian distribution is observed in the boundary-layer atmosphere during wind storm events, especially typhoons or hurricanes. For the turbulence-induced vibration, traditional Gaussian assumption may lead to non-conservative results, especially for non-Gaussian turbulence with positive skewness. Based on the state augmentation method, this paper derives formulations to calculate the moments of buffeting response. The non-Gaussian turbulence-induced buffeting forces are approximated by Hermite polynomials of the underlying Gaussian process, modeled as Ornstein–Uhlenbeck process in the state augmentation method. The state augmentation method is verified for bridge buffeting vibration caused by Gaussian turbulence, and the approximation of buffeting force by the Ornstein–Uhlenbeck process is also validated. Applying the state augmentation method on the bridge buffeting response excited by non-Gaussian turbulence, the corresponding bridge buffeting response RMS, skewness and kurtosis can be computed sequentially. The results show that the RMS of buffeting responses induced by non-Gaussian turbulence is slightly higher than Gaussian turbulence results. However, the extreme responses are greatly affected by the skewness of non-Gaussian turbulence.

1. Introduction

Wind-induced vibration is a long-lasting wind engineering research topic for flexible structures, such as long-span bridges, large-span roofs, and skyscrapers. Pioneeringly, Prof. Alan Davenport established the wind-induced vibration calculation procedure through the sequential analysis of wind climate field, bluff-body aerodynamics, and structural dynamics [1]. Later, this approach has been summarized as the famous "Davenport Chain" [2] and widely used to perform the structural wind effects evaluation in modern wind engineering applications.

In the beginning, for the turbulence-induced vibration, Davenport established the structural buffeting evaluation method in frequency domain based on statistics and stochastic vibration theory [3]. It can be summarized as the PSD (power spectral density) of structural response can be calculated through a sequential multiplication of turbulence PSD, aerodynamic admittance and mechanical admittance. For line-shaped structures, such as tall buildings and long-span bridges, the aerodynamic admittance normally depends on mean wind speeds and span-wise turbulence coherence; for thin plate structural section, such as bridge deck, the chord-wise aerodynamic admittance also should be considered. The structural admittance can be derived from the structural dynamic transfer function [4]. This theory has been widely used for tall buildings buffeting response [5–7], suspended cables [8] and other vertical structures [9].

Next, the bridge section self-excited aerodynamic forces was found to be important for bridge buffeting response [10] because the motion dependent aero-damping and aero-stiffness can greatly affect the structural dynamic properties. It was proposed that the buffeting analysis should consider turbulence-induced aerodynamic force as the excitation and motion-induced aeroelastic force as the system properties. Meanwhile, the flexible long-span bridge is one particular type of structure with very closely spaced dynamic mode frequencies; thus, multiple modes coupling effects caused by aero-damping and aero-stiffness must be included to calculate wind-induced bridge buffeting responses.

* Correspondence to: 305 Wind Engineering Building, Tongji University, 1239 Siping Road, Shanghai, 200092, China.
E-mail addresses: cuiwei@tongji.edu.cn (W. Cui), zhaolin@tongji.edu.cn (L. Zhao), yaojunge@tongji.edu.cn (Y. Ge).

https://doi.org/10.1016/j.engstruct.2021.113774
Received 22 September 2021; Received in revised form 2 December 2021; Accepted 17 December 2021
Available online 21 January 2022

Nomenclature

$\boldsymbol{A}$	State matrix
$\boldsymbol{A}_1$, $\boldsymbol{A}_2$, $\boldsymbol{A}_3$, $\boldsymbol{A}_{l+3}$	Frequency independent flutter derivatives
$\boldsymbol{B}$	Input matrix
$\bar{\boldsymbol{C}}$	Net damping matrix
$\boldsymbol{C}_q$	Modal generalized damping matrix
$\boldsymbol{C}$	Damping matrix
$\boldsymbol{F}_{\mathrm{b}}$	Buffeting forces array
$\boldsymbol{F}_{\mathrm{se}}$	Self-excited aerodynamic forces array
$\bar{\boldsymbol{K}}$	Net stiffness matrix
$\boldsymbol{K}_q$	Modal generalized stiffness matrix
$\boldsymbol{K}$	Stiffness matrix
$\bar{\boldsymbol{M}}$	Net mass matrix
$\boldsymbol{M}_q$	Modal generalized Mass matrix
$\boldsymbol{M}$	Mass matrix
$\boldsymbol{Q}_{\mathrm{b}}$	Modal generalized buffeting forces array
$\boldsymbol{Q}_{\mathrm{se}}$	Modal generalized Self-excited aerodynamic forces array
$\boldsymbol{R}_{ZZ}$	Auto-covariance of $\boldsymbol{Z}$
$\boldsymbol{S}_{ZZ}$	PSD of $\boldsymbol{Z}$
$\boldsymbol{S}_{\tilde{Z}\tilde{Z}}$	PSD of $\tilde{\boldsymbol{Z}}$
$\boldsymbol{S}_{u,w}$	PSD matrix of turbulence
$\boldsymbol{W}$	Wiener process (Standard Brownian motion)
$\boldsymbol{X}$	State vector including Gaussian buffeting forces
$\boldsymbol{Y}$	State vector
$\boldsymbol{Z}$	Gaussian buffeting forces approximated by Ornstein-Uhlenbeck process
$\boldsymbol{d}$	Displacements array
$\boldsymbol{g}(\boldsymbol{X},t)$	Drift vector in Itô equation
$\boldsymbol{h}(\boldsymbol{X},t)$	Diffusion matrix in Itô equation
$\boldsymbol{q}$	Modal generalized coordinates
$\bigtriangledown_{\boldsymbol{X}}\xi$	Gradient of ξ with respect to $\boldsymbol{X}$
$\tilde{\boldsymbol{Z}}$	Underlying multi-variate Gaussian buffeting forces vector
$\boldsymbol{\Phi}$	Modal shapes matrix
$\boldsymbol{\alpha}$	Time relaxing coefficients matrix
$\mathbb{K}$	Covariance matrix of $\boldsymbol{Z}$
$\boldsymbol{\Theta}$	Diffusing matrix
$\boldsymbol{\phi}_l$	Aerodynamic phase lag matrix
A_i^* $(i=1\sim6)$	Torsional flutter derivatives
B	Bridge deck width
C_D	Drag coefficient
C_D'	Derivative of Drag coefficient in term of angle of attack
C_L	Lift coefficient
C_L'	Derivative of Lift coefficient in term of angle of attack
C_M	Torque coefficient
C_M'	Derivative of Torque coefficient in term of angle of attack
C_{uu}	Coherence function of along-wind turbulence along span direction
C_{ww}	Coherence function of vertical turbulence along span direction
D_{b}	Aerodynamic buffeting drag forces
D_{se}	Self-excited aerodynamic drag forces
H_i^* $(i=1\sim6)$	Vertical flutter derivatives
$H_{\boldsymbol{X}}\xi$	Hessian matrix of ξ with respect to $\boldsymbol{X}$
I_u, I_w	Turbulence intensity of u and w
K	Hermit polynomial expansion order
L_u, L_w	Turbulence integral length of u and w
L_{b}	Aerodynamic buffeting lift forces
L_{se}	Self-excited aerodynamic lift forces
M_{b}	Aerodynamic buffeting torque
M_{se}	Self-excited aerodynamic torque
P_i^* $(i=1\sim6)$	Lateral flutter derivatives
S_{uu}	PSD of along-wind turbulence
S_{ww}	PSD of vertical turbulence
Tr[ ]	Trace Operator
U	Mean wind speed
a_1	Moment order of displacement at 1st DOF (vertical)
a_2	Moment order of displacement at 2nd DOF (torsional)
b_1	Moment order of displacement at 1st DOF (vertical)
b_2	Moment order of velocity at 2nd DOF (torsional)
d_l	Self-excited force phase delay
f_1	Moment order of buffeting force at 1st DOF (vertical)
f_2	Moment order of buffeting force at 2nd DOF (torsional)
h	Vertical displacement
h_α	Peak factor of torsional response
$h_{\max,\gamma}$	Extreme vertical vibration caused by non-Gaussian turbulence with skewness γ
$h_{\max}$	Extreme vertical response
i	Flutter derivatives index $(i=1\sim6)$
j	DOF index
k	Hermit polynomial expansion index
l	Aeroelastic force expansion index
m	Aeroelastic force expansion order
$m(\ )$	Moments function of $\boldsymbol{X}$
n	DOF number
p	Lateral displacement
r, s	Looping index in vector $\boldsymbol{X}$
u	Along-wind wind speed component
w	Vertical wind speed component
$\mathfrak{C}$	Aerodynamic coefficients matrix
$\mathfrak{g}_k$	Hermit polynomial coefficients array
$\mathbb{h}_3$, $\mathbb{h}_4$, $\mathbb{k}$	Hermite polynomial coefficients of buffeting response

An elegant formulation considering the multi-mode coupling effect was proposed based on dimensionless frequency and time to calculate both the flutter and buffeting response for long-span bridges [11]. In modern bridge construction practice, non-uniform section shapes and properties for super-long-span, therefore, location-dependent structural and aeroelastic properties can also be integrated with mode shapes along the span direction in the above method, which was applied to Akashi Kaikyo Bridge in Japan [12]. On the other hand, the vibration control techniques using TMD [13,14] were also investigated on long-span bridges.

As the development of the computer hardware in recent decades, the time-domain method became an alternative and powerful tool

$\mathbb{s}$	Order of moments function $m(a_1, a_2, b_1, b_2, f_1, f_2)$
α	Torsional displacement
$\alpha_{\max,\gamma}$	Extreme torsional vibration caused by non-Gaussian turbulence with skewness γ
$\alpha_{\max}$	Extreme torsional response
γ_e	Euler constant
γ_h	Skewness of vertical response
γ_α	Skewness of torsional response
$\gamma_{u,w}$	Skewness of non-Gaussian turbulence
$\imath$	Unit virtual number
κ	Reduced frequency
κ_α	Kurtosis of torsional response
ρ	Air density
σ_h	RMS of vertical response
$\sigma_{\alpha,\gamma}$	RMS of torsional vibration caused by non-Gaussian turbulence with skewness γ
σ_α	RMS of torsional response
$\sigma_{h,\gamma}$	RMS of vertical vibration caused by non-Gaussian turbulence with skewness γ
τ	Time delay
ω	Circular frequency
$\chi_{L_{bu}}$, $\chi_{L_{bw}}$, $\chi_{D_{bu}}$, $\chi_{D_{bu}}$, $\chi_{M_{bu}}$, $\chi_{M_{bw}}$	Aerodynamic admittance functions
$\xi(\ )$	Arbitrary numerical function of $\boldsymbol{X}$ at time t

to perform bridge buffeting analysis with multi-source nonlinearity including geometry, material, and aeroelastic. The key of time-domain method is to use the indicial function from aerospace engineering to evaluate the self-excited motion-dependent aeroelastic forces along the bridge deck [15]. The rational function approximation approach is employed to approximate the unsteady aeroelastic force, which is also known as Roger's approximation [16].

However, the first step of the time-domain simulation is the numerical generation of random turbulence time series, which unavoidably incorporates randomness from wind field to structural responses. Thus, the simulation results are not identical even all parameters keep the same for different implementations of random field generation. In contrast, for frequency domain analysis, because the randomness of turbulent wind can be presented by the statistical characters distributed over the frequency domain, the structural responses are evaluated determinately at each frequency point. Nevertheless, the application of frequency-domain analysis requires a linear dynamic system, and the excitation has to follow Gaussian distribution.

In recent years, with the massive deployment of high-frequency wind field monitoring devices, such as ultrasonic anemometer, more deeper characteristics of turbulence in the atmosphere boundary layer have been observed. Several studies state that the wind turbulence sometimes does not follow Gaussian assumption [17,18]. In contrast, the non-Gaussian turbulence in the wind fields has been reported in several studies [19], but the related dynamic effect through the wind-force-response Davenport's wind loading chain has been less concerned for wind sensitive structures.

At the same time, the wind pressure is naturally non-Gaussian because of the quadratic term of turbulence [20] and wind flow separation on large roof edges [21]. Several methods have been developed to derive the higher-order moment of structural response at time-domain [22] and frequency domain [20]. In wind engineering applications, the quadratic term of turbulence is insignificant due to small turbulence intensity [23]. Thus, the Gaussian assumption of turbulence is widely used for turbulent wind-induced vibration.

However, when the turbulence does not follow Gaussian distribution in a particular situation, the traditional second-order frequency domain analysis is invalid, and the development of complex high-order bi-spectrum and tri-spectrum is required. On the other hand, though time domain analysis [24] can calculate structural responses excited by non-Gaussian turbulence with even non-linear aeroelastic force, the substantial demanding computational resources and unavoidable calculation randomness restrict its application on complex structures. Vanmarcke's approaches [25] can be employed for the structural dynamic analysis when the turbulent wind is implemented in nonstationary perspective.

When the random structural excitation can be expressed as a summation of polynomials, *Grigoriu* developed a moment equations based on Itô lemma to calculate the responses moments to different orders for single degree of freedom (DOF) system [26]. Later, this approach had been summarized as the state augmentation method in [27]. Recently, this method is used to derive the turbulence-induced vibration of simply supported thin flat plate [28] considering the quadratic term in wind pressure. However, only single-degree freedom systems were considered in the above two studies because of the modes orthogonality. Furthermore, For nonlinear dynamic system, the moments closure method is required to approximate the moments of dynamic states.

In engineering practice, non-Gaussian turbulence [29] can be approximated as the summation of Hermite polynomials [30–32]. Therefore, applying the state augmentation method to structures subjected to non-Gaussian turbulence with single degree of freedom is straightforward, such as point-like structures and continuum structures after mode decomposition. However, for the flexible structures affected by aeroelastic, the aeroelastic damping matrix is normally non-classic [33], such as long-span bridge [34] and tall building with irregular sectional shape [23]. Consequently, the state augmentation formulations established for the single DOF system should be expanded to multiple DOFs (MDOF).

This paper first derives the MDOF formulation for stochastic vibrations of long-span bridges induced by non-Gaussian turbulence based on the state augmentation method. Then, this formulation is verified through comparison against the frequency domain method when random excitation is Gaussian. At last, the effect of skewness of non-Gaussian turbulence-induced bridge vibration is investigated. In summary, this paper provides an alternative approach to calculate long-span bridge buffeting response subjected to non-Gaussian turbulence, besides the traditional time-domain approach.

2. State augmentation formulations of non-Gaussian turbulence induced buffeting for long-span bridges

2.1. State space equation of bridge motion

The governing equation of bridge deck motion in continuum structure is normally expressed as:

$$\boldsymbol{M}\ddot{\boldsymbol{d}} + \boldsymbol{C}\dot{\boldsymbol{d}} + \boldsymbol{K}\boldsymbol{d} = \boldsymbol{F}_{\mathrm{se}} + \boldsymbol{F}_{\mathrm{b}} \tag{1}$$

in which $\boldsymbol{M}$ is the mass matrix, $\boldsymbol{C}$ is the damping matrix and $\boldsymbol{K}$ is the stiffness matrix; $\boldsymbol{d}$ is the motion array consisting of the displacements at three DOFs: sway direction (horizontal) p, hovering direction (vertical) h and pitching (rotation) α.

For long-span bridges, there are two types of external excitation forces $\boldsymbol{F}$: self-motion-excited aeroelastic force $\boldsymbol{F}_{\mathrm{se}}$ and turbulence induced random aerodynamic force $\boldsymbol{F}_{\mathrm{b}}$. Both of them have three directional components: drag force D_{se} and D_{b}, lift force L_{se} and L_{b} and torque M_{se} and M_{b}.

Fig. 1 illustrates the external force and motion per unit span on bridge section.

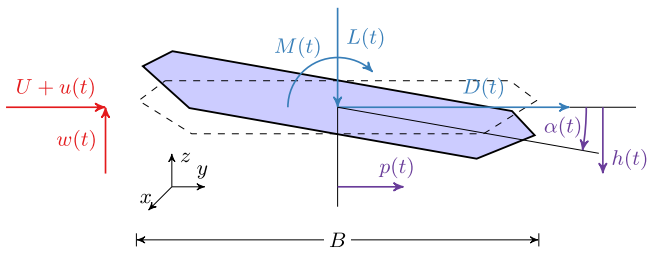

Fig. 1. Two coordinates system about aerodynamic force and bridge motion (The notations can be found in Eq. (1)).

If the bridge section vibrates in harmonic motion, the self-excited forces are commonly described by Scanlan's flutter derivatives:

$$D_{se} = \frac{1}{2}\rho U^2 B\left(\kappa P_1^*\frac{\dot{p}}{U} + \kappa P_2^*\frac{B\dot{\alpha}}{U} + \kappa^2 P_3^*\alpha + \kappa^2 P_4^*\frac{p}{B} + \kappa P_5^*\frac{\dot{h}}{U} + \kappa^2 P_6^*\frac{h}{B}\right) \tag{2a}$$

$$L_{se} = \frac{1}{2}\rho U^2 B\left(\kappa H_1^*\frac{\dot{h}}{U} + \kappa H_2^*\frac{B\dot{\alpha}}{U} + \kappa^2 H_3^*\alpha + \kappa^2 H_4^*\frac{h}{B} + \kappa H_5^*\frac{\dot{p}}{U} + \kappa^2 H_6^*\frac{p}{B}\right) \tag{2b}$$

$$M_{se} = \frac{1}{2}\rho U^2 B^2\left(\kappa A_1^*\frac{\dot{h}}{U} + \kappa A_2^*\frac{B\dot{\alpha}}{U} + \kappa^2 A_3^*\alpha + \kappa^2 A_4^*\frac{h}{B} + \kappa A_5^*\frac{\dot{p}}{U} + \kappa^2 A_6^*\frac{p}{B}\right) \tag{2c}$$

where ρ is air density; U is the mean wind speeds; $\kappa = \omega B/U$ is the reduced frequency; B is the bridge deck width; ω is the circular frequency; H_i^*, P_i^* and A_i^* ($i = 1 \sim 6$) are frequency dependent flutter derivatives.

Eq. (2) can be transformed by Laplace transformation into frequency domain in matrix form as:

$$\begin{Bmatrix} D_{se} \\ L_{se} \\ M_{se} \end{Bmatrix} = \frac{1}{2}\rho U^2 \begin{bmatrix} B & & \\ & B & \\ & & B^2 \end{bmatrix} \times \begin{bmatrix} \kappa^2(P_4^* + \imath P_1^*) & \kappa^2(P_6^* + \imath P_5^*) & \kappa^2(P_3^* + \imath P_2^*) \\ \kappa^2(H_6^* + \imath H_5^*) & \kappa^2(H_4^* + \imath H_1^*) & \kappa^2(H_3^* + \imath H_2^*) \\ \kappa^2(A_6^* + \imath A_5^*) & \kappa^2(A_4^* + \imath A_1^*) & \kappa^2(A_3^* + \imath A_2^*) \end{bmatrix} \begin{Bmatrix} p/B \\ h/B \\ \alpha \end{Bmatrix} \tag{3}$$

where $\imath$ is the imaginary unit $\imath^2 = -1$.

In Eq. (3), the flutter derivative matrix can be approximated by rational function [35]:

$$\begin{bmatrix} \kappa^2(P_4^* + \imath P_1^*) & \kappa^2(P_6^* + \imath P_5^*) & \kappa^2(P_3^* + \imath P_2^*) \\ \kappa^2(H_6^* + \imath H_5^*) & \kappa^2(H_4^* + \imath H_1^*) & \kappa^2(H_3^* + \imath H_2^*) \\ \kappa^2(A_6^* + \imath A_5^*) & \kappa^2(A_4^* + \imath A_1^*) & \kappa^2(A_3^* + \imath A_2^*) \end{bmatrix} = \boldsymbol{A}_1 + \boldsymbol{A}_2(\imath\kappa) + \boldsymbol{A}_3(\imath\kappa)^2 + \sum_{l=1}^{m}\frac{\boldsymbol{A}_{l+3}\imath\kappa}{\imath\kappa + d_l} \tag{4}$$

in which m is the aeroelastic force expansion order, the frequency independent variables $\boldsymbol{A}_1$, $\boldsymbol{A}_2$, $\boldsymbol{A}_3$, $\boldsymbol{A}_{l+3}$ and d_l can be determined by nonlinear least square method. It should be noted that rational approximation may become less efficient when the more phase lags are required for non-negligible vortex shedding effect.

Next, through inverse Laplace transformation, the self-excited force is re-transformed as:

$$\begin{Bmatrix} D_{se} \\ L_{se} \\ M_{se} \end{Bmatrix} = \frac{1}{2}\rho U^2 \begin{bmatrix} B & & \\ & B & \\ & & B^2 \end{bmatrix} \left[\boldsymbol{A}_1\boldsymbol{d} + \boldsymbol{A}_2\frac{B}{U}\dot{\boldsymbol{d}} + \boldsymbol{A}_3\frac{B^2}{U^2}\ddot{\boldsymbol{d}} + \sum_{l=1}^{m}\boldsymbol{\phi}_l(t)\right] \tag{5a}$$

$$\dot{\boldsymbol{\phi}}_l(t) = -\frac{d_l U}{B}\boldsymbol{\phi}_l(t) + \boldsymbol{A}_{l+3}\dot{\boldsymbol{d}} \tag{5b}$$

where $\boldsymbol{\phi}_l(t)$ is the phase lag to describe aerodynamic memory effect. When the number of phase lag terms is large for non-streamlined bridge section, extra DOFs should be brought into the state augmentation formula proposed following.

The turbulence induced buffeting force per unit span are normally expressed as:

$$D_b(t) = \frac{1}{2}\rho U^2 B\left[2C_D\chi_{D_{bu}}\frac{u(t)}{U} + C_D'\chi_{D_{bw}}\frac{w(t)}{U}\right] \tag{6a}$$

$$L_b(t) = \frac{1}{2}\rho U^2 B\left[2C_L\chi_{L_{bu}}\frac{u(t)}{U} + (C_L' + C_D)\chi_{L_{bw}}\frac{w(t)}{U}\right] \tag{6b}$$

$$M_b(t) = \frac{1}{2}\rho U^2 B^2\left[2C_M\chi_{M_{bu}}\frac{u(t)}{U} + C_M'\chi_{M_{bw}}\frac{w(t)}{U}\right] \tag{6c}$$

where C_L, C_D and C_M are lift, drag and moment coefficients, respectively; $C_D' = \frac{dC_D}{d\alpha}$, $C_L' = \frac{dC_L}{d\alpha}$ and $C_M' = \frac{dC_M}{d\alpha}$; $\chi_{L_{bu}}$, $\chi_{L_{bw}}$, $\chi_{D_{bu}}$, $\chi_{D_{bw}}$, $\chi_{M_{bu}}$ and $\chi_{M_{bw}}$ are aerodynamic admittance functions, which are frequency dependent.

For structures with linear mechanical properties, modal decomposition and superposition is employed to increase computational efficiency through reduce order of DOFs.

$$\boldsymbol{M}_q\ddot{\boldsymbol{q}} + \boldsymbol{C}_q\dot{\boldsymbol{q}} + \boldsymbol{K}_q\boldsymbol{q} = \boldsymbol{Q}_{se} + \boldsymbol{Q}_b \tag{7}$$

where $\boldsymbol{M}_q = \boldsymbol{\Phi}^T\boldsymbol{M}\boldsymbol{\Phi}$, $\boldsymbol{C}_q = \boldsymbol{\Phi}^T\boldsymbol{C}\boldsymbol{\Phi}$ and $\boldsymbol{K}_q = \boldsymbol{\Phi}^T\boldsymbol{K}\boldsymbol{\Phi}$ are modal generalized mass, damping and stiffness; $\boldsymbol{Q}_{se} = \boldsymbol{\Phi}^T\boldsymbol{F}_{se}$, $\boldsymbol{Q}_b = \boldsymbol{\Phi}^T\boldsymbol{F}_b$ are generalized self-excited and buffeting force respectively; $\boldsymbol{\Phi}$ is mode shape matrix. The transformation of aeroelastic forces from conventional coordinates to dynamic model coordinates requires that each mode shape has only one motion component (lateral, vertical or torsional). Coupled motion in mode shapes may cause inaccurate bridge buffeting calculating results.

Finally, the above generalized motion equation can be expressed in state-space equation:

$$\dot{\boldsymbol{Y}} = \boldsymbol{A}\boldsymbol{Y} + \boldsymbol{B}\boldsymbol{Q}_b \tag{8}$$

where

$$\boldsymbol{Y} = \begin{Bmatrix} \boldsymbol{q} \\ \dot{\boldsymbol{q}} \\ \boldsymbol{q}_{se,1} \\ \vdots \\ \boldsymbol{q}_{se,m} \end{Bmatrix} \tag{9a}$$

$$\boldsymbol{A} = \begin{bmatrix} \boldsymbol{0} & \boldsymbol{I} & \boldsymbol{0} & \cdots & \boldsymbol{0} \\ -\bar{\boldsymbol{M}}^{-1}\bar{\boldsymbol{K}} & -\bar{\boldsymbol{M}}^{-1}\bar{\boldsymbol{C}} & \frac{1}{2}\rho U^2\bar{\boldsymbol{M}}^{-1} & \cdots & \frac{1}{2}\rho U^2\bar{\boldsymbol{M}}^{-1} \\ \boldsymbol{0} & \boldsymbol{A}_{4,q} & -\frac{U}{B}d_1\boldsymbol{I} & \cdots & \boldsymbol{0} \\ \vdots & \vdots & \vdots & \ddots & \vdots \\ \boldsymbol{0} & \boldsymbol{A}_{3+m,q} & \boldsymbol{0} & \cdots & -\frac{U}{B}d_m\boldsymbol{I} \end{bmatrix} \tag{9b}$$

$$\boldsymbol{B} = \begin{bmatrix} \boldsymbol{0} \\ \bar{\boldsymbol{M}}^{-1} \\ \boldsymbol{0} \\ \vdots \\ \boldsymbol{0} \end{bmatrix} \tag{9c}$$

$$\bar{\boldsymbol{M}} = \boldsymbol{M}_q - \frac{1}{2}\rho B^2\boldsymbol{A}_{3,q} \tag{9d}$$

$$\bar{\boldsymbol{C}} = \boldsymbol{C}_q - \frac{1}{2}\rho BU\boldsymbol{A}_{2,q} \tag{9e}$$

$$\bar{\boldsymbol{K}} = \boldsymbol{K}_q - \frac{1}{2}\rho U^2\boldsymbol{A}_{1,q} \tag{9f}$$

where $\boldsymbol{A}_{i,q} = \boldsymbol{\Phi}^T\boldsymbol{A}_i\boldsymbol{\Phi}$ ($i = 1 \sim m$) is generalized aerodynamic frequency independent coefficients.

Table 1
Consistent structural parameters of six bridge models.

Parameters	Values
Main span	1263
Sag–span ratio	1/11
Deck width B (m)	27.63
Deck thickness D (m)	4
Suspenders gap (m)	20
Mass per unit length M (kg/m)	40 000
Mass moment of inertia long longitudinal axis per unit length I (kg m^2/m)	4 483 763
Area of bridge section (m^2)	1.11
Area moment of inertia $I_x/I_y/I_z$ (m^4)	5.5/2.64/94
Structural damping ratio	0.005
Air density ρ (kg/m^3)	1.25
Lift coefficient C_L	0.0942
Drag coefficient C_D	0.3042
Moment coefficient C_M	0.0104
Lift coefficient derivative $dC_L/d\alpha$	1.9050
Drag coefficient derivative $dC_D/d\alpha$	0
Moment coefficient derivative $dC_M/d\alpha$	0.2717

The generalized buffeting force can be expanded as:

$$\begin{aligned}\boldsymbol{Q}_{\mathrm{b}} = \boldsymbol{\Phi}^T \boldsymbol{F}_{\mathrm{b}} &= \int_0^l \begin{bmatrix} \phi_{1,z}(x) & \phi_{1,y}(x) & \phi_{1,x}(x) \\ \phi_{2,z}(x) & \phi_{2,y}(x) & \phi_{2,x}(x) \\ & \cdots & \\ \phi_{j,z}(x) & \phi_{j,y}(x) & \phi_{j,x}(x) \\ & \cdots & \\ \phi_{n,z}(x) & \phi_{n,y}(x) & \phi_{n,x}(x) \end{bmatrix} \begin{Bmatrix} D_{\mathrm{b}}(x;t) \\ L_{\mathrm{b}}(x;t) \\ M_{\mathrm{b}}(x;t) \end{Bmatrix} dx \\ &= \frac{1}{2}\rho U \int_0^l \boldsymbol{\Phi}^T(x) \begin{bmatrix} 2C_D\chi_{D_{bu}} & C'_D\chi_{D_{bw}} \\ 2C_L\chi_{L_{bu}} & (C'_L+C_D)\chi_{L_{bw}} \\ 2C_M\chi_{M_{bu}} & C'_M\chi_{M_{bw}} \end{bmatrix} \begin{Bmatrix} u(x;t) \\ w(x;t) \end{Bmatrix} dx \end{aligned} \tag{10}$$

where n is the number of bridge structural modes interested.

The PSD of $\boldsymbol{Q}_{\mathrm{b}}$ is:

$$\begin{aligned} S_{\boldsymbol{Q}_{\mathrm{b}}\boldsymbol{Q}_{\mathrm{b}}}(\omega) = \left(\frac{1}{2}\rho U\right)^2 \iint_0^l \boldsymbol{\Phi}^T(x_1)\mathbb{C}^T(\omega)\boldsymbol{S}_{u,w}(x_1,x_2;\omega) \\ \times \mathbb{C}(\omega)\boldsymbol{\Phi}(x_2)dx_1dx_2 \end{aligned} \tag{11}$$

in which

$$\mathbb{C}(\omega) = \begin{bmatrix} 2C_D\chi_{D_{bu}}(\omega) & 2C_L\chi_{L_{bu}}(\omega) & 2C_M\chi_{M_{bu}}(\omega) \\ C'_D\chi_{D_{bw}}(\omega) & (C'_L+C_D)\chi_{L_{bw}}(\omega) & C'_M\chi_{M_{bw}}(\omega) \end{bmatrix} \tag{12a}$$

$$\begin{aligned} \boldsymbol{S}_{u,w}(x_1,x_2;\omega) &= \begin{bmatrix} S_{uu}(x_1,x_2;\omega) & 0 \\ 0 & S_{ww}(x_1,x_2;\omega) \end{bmatrix} \\ &= \begin{bmatrix} S_{uu}(\omega) & 0 \\ 0 & S_{ww}(\omega) \end{bmatrix} \begin{bmatrix} C_{uu}(x_1,x_2;\omega) & 0 \\ 0 & C_{ww}(x_1,x_2;\omega) \end{bmatrix} \end{aligned} \tag{12b}$$

$$C_{uu}(x_1,x_2;\omega) = \exp\left(-\frac{c_u\omega|x_1-x_2|}{2\pi U}\right) \tag{12c}$$

$$C_{ww}(x_1,x_2;\omega) = \exp\left(-\frac{c_w\omega|x_1-x_2|}{2\pi U}\right) \tag{12d}$$

2.2. Moments function of bridge motion subjected to non-Gaussian turbulence

When the turbulence u and w are non-Gaussian processes, their skewness and kurtosis can be directly transferred to the buffeting forces due to the linear relationship presented in Eq. (10). Thus $\boldsymbol{Q}_{\mathrm{b}}(t)$ can be approximated as polynomials of underlying Gaussian process $\tilde{\boldsymbol{Z}}(t)$:

$$\boldsymbol{Q}_{\mathrm{b}}(t) = \sum_{k=0}^{K} \mathbf{g}_k \tilde{\boldsymbol{Z}}^k(t) \tag{13}$$

in which $\mathbf{g}_k$ is Hermit polynomial coefficients array and K is the Hermit polynomial expansion order. $\tilde{\boldsymbol{Z}}(t)$ is multi-variate process vector with standard Gaussian distribution, and $\mathbf{g}_k$ and $\boldsymbol{S}_{\tilde{Z}\tilde{Z}}$ can be found using the spectrum distortion method in [30].

In this study, the multivariate Ornstein–Uhlenbeck processes shown in Eq. (14) is employed to approximate the underlying buffeting forces array $\boldsymbol{Z}(t) \approx \tilde{\boldsymbol{Z}}(t)$.

$$d\boldsymbol{Z} = -\boldsymbol{\alpha}\boldsymbol{Z}dt + \boldsymbol{\Theta}d\boldsymbol{W}(t) \tag{14}$$

in which $\boldsymbol{\alpha}$ is the time relaxing coefficients array, $\boldsymbol{\Theta}$ is diffusing matrix of $\boldsymbol{Z}(t)$ and $d\boldsymbol{W}(t)$ is independent multi-dimensional Wiener process. The multivariate Ornstein–Uhlenbeck processes employed in this study is equivalent as the approximation of red color noise linearly transformed from Wiener process [36]. $\boldsymbol{\alpha}$ can be found through fitting the covariance matrix of $\boldsymbol{Z}$ expressed as $\boldsymbol{R}_{ZZ}(\tau) = \exp(-\boldsymbol{\alpha}|\tau|)\mathbb{K}$, where $\mathbb{K}$ is the covariance matrix of $\boldsymbol{Z}$ which is equivalent to $\boldsymbol{R}_{ZZ}(0)$ and $\boldsymbol{R}_{ZZ}(\tau)$ is derived from inverse Fourier transformation of $\boldsymbol{S}_{ZZ}$.

$\boldsymbol{\Theta}$ is determined from

$$\boldsymbol{\Theta}\boldsymbol{\Theta}^T = \boldsymbol{\alpha}\mathbb{K} + \mathbb{K}\boldsymbol{\alpha}^T \tag{15}$$

From Eq. (8), Eqs. (13) and (14), the augmented state of structural buffeting response can be reorganized as:

$$\begin{aligned} d\begin{bmatrix} \boldsymbol{q}(t) \\ \dot{\boldsymbol{q}}(t) \\ \boldsymbol{q}_{\mathrm{se}}(t) \\ \boldsymbol{Z}(t) \end{bmatrix} &= \begin{bmatrix} \boldsymbol{0} & \boldsymbol{I} & \boldsymbol{0} & \boldsymbol{0} \\ -\bar{\boldsymbol{M}}^{-1}\bar{\boldsymbol{K}} & -\bar{\boldsymbol{M}}^{-1}\bar{\boldsymbol{C}} & \frac{1}{2}\rho U^2\bar{\boldsymbol{M}}_+^{-1} & \bar{\boldsymbol{M}}^{-1}\sum_{k=0}^{K}\mathbf{g}_k\boldsymbol{Z}^{k-1}(t) \\ \boldsymbol{0} & \boldsymbol{A}_{4+,q} & -\frac{U}{B}\boldsymbol{d}_{se} & \boldsymbol{0} \\ \boldsymbol{0} & \boldsymbol{0} & \boldsymbol{0} & -\boldsymbol{\alpha} \end{bmatrix} \\ &\times \begin{bmatrix} \boldsymbol{q}(t) \\ \dot{\boldsymbol{q}}(t) \\ \boldsymbol{q}_{\mathrm{se}}(t) \\ \boldsymbol{Z}(t) \end{bmatrix} dt + \begin{bmatrix} \boldsymbol{0} \\ \boldsymbol{0} \\ \boldsymbol{0} \\ \boldsymbol{\Theta} \end{bmatrix} d\boldsymbol{W}(t) \end{aligned} \tag{16}$$

in which

$$\bar{\boldsymbol{M}}_+^{-1} = \begin{bmatrix} \bar{\boldsymbol{M}}^{-1} & \cdots & \bar{\boldsymbol{M}}^{-1} \end{bmatrix} \tag{17a}$$

$$\boldsymbol{A}_{4+,q} = \begin{bmatrix} \boldsymbol{A}_{3+1,q} \\ \vdots \\ \boldsymbol{A}_{3+m,q} \end{bmatrix} \tag{17b}$$

$$\boldsymbol{d}_{se} = \mathrm{diag}\begin{bmatrix} d_1\boldsymbol{I} & \cdots & d_m\boldsymbol{I} \end{bmatrix} \tag{17c}$$

The Eq. (16) can be written in standardized Itô equation:

$$d\boldsymbol{X}(t) = \boldsymbol{g}(\boldsymbol{X}(t),t)\,dt + \boldsymbol{h}(\boldsymbol{X}(t),t)\,d\boldsymbol{W}(t) \tag{18}$$

Let $\xi(\boldsymbol{X}(t),t)$ be a scalar function of the $(3n+m)$-dimensional state vector $\boldsymbol{X}(t)$ and time t. According to Itô's lemma [37],

$$d\xi = \left\{\frac{\partial\xi}{\partial t} + \left(\nabla_{\boldsymbol{X}}\xi\right)^T\boldsymbol{g} + \frac{1}{2}\mathrm{Tr}\left[\boldsymbol{h}^T(H_{\boldsymbol{X}}\xi)\boldsymbol{h}\right]\right\}dt + \left(\nabla_{\boldsymbol{X}}\xi\right)^T\boldsymbol{h}d\boldsymbol{W} \tag{19}$$

where $\nabla_{\boldsymbol{X}}\xi$ is the gradient of ξ with respect to $\boldsymbol{X}$, $H_{\boldsymbol{X}}\xi$ is the Hessian matrix of ξ with respect to $\boldsymbol{X}$ and Tr[ ] is the Trace Operator.

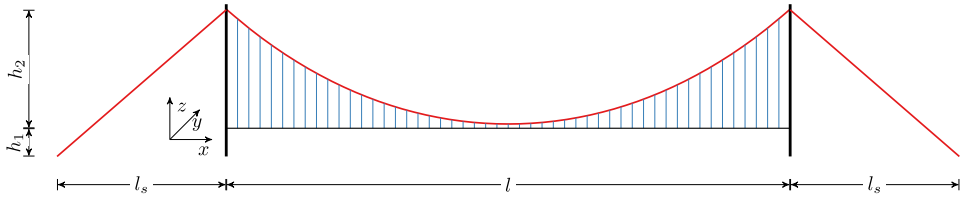

Fig. 2. Sketch of long-span suspension bridge.

According to [38], the expectation of above equation is

$$\frac{d\mathbb{E}[\xi]}{dt} = \mathbb{E}\left[\frac{\partial \xi}{\partial t}\right] + \sum_{r}^{3n+m} \mathbb{E}\left[\frac{\partial \xi}{\partial X_r} g_r\right] + \frac{1}{2}\sum_{r,s}^{3n+m} \mathbb{E}\left[\left(\boldsymbol{h}\boldsymbol{h}^T\right)_{rs} \frac{\partial^2 \xi}{\partial X_r \partial X_s}\right] \tag{20}$$

Let $\xi = m(\,)$, which is the function of augumented state vector $\boldsymbol{X}(t)$ defined as:

$$\begin{aligned}\xi &= m(a_1, \ldots, a_n, b_1, \ldots, b_n, e_1, \ldots, e_m, f_1, \ldots, f_n; t) \\ &= \prod_{j=1}^{n} q_j^{a_j} \prod_{j=1}^{n} \dot{q}_j^{b_j} \prod_{l=1}^{m} q_{\mathrm{se},l}^{e_l} \prod_{j=1}^{n} Z_j^{f_j}\end{aligned} \tag{21}$$

in which a_j, b_j, e_l and f_j are non-negative integers.

Substitute Eq. (21) into Eq. (20),

$$\begin{aligned}&\frac{d\mathbb{E}\left[m(a_1, \ldots, a_n, b_1, \ldots, b_n, e_1, \ldots, e_m, f_1, \ldots, f_n; t)\right]}{dt} \\ &= \mathbb{E}\left[\frac{\partial m(a_1, \ldots, a_n, b_1, \ldots, b_n, e_1, \ldots, e_m, f_1, \ldots, f_n; t)}{\partial t}\right] \\ &+ \sum_{r=1}^{n} a_r \mathbb{E}\left[\prod_{j=1}^{n} q_j^{a_j} \prod_{j=1}^{n} \dot{q}_j^{b_j} \prod_{l=1}^{m} q_{\mathrm{se},l}^{e_l} \prod_{j=1}^{n} Z_j^{f_j} \cdot q_r^{-1} g_r\right] \\ &+ \sum_{r=n+1}^{2n} b_{r-n} \mathbb{E}\left[\prod_{j=1}^{n} q_j^{a_j} \prod_{j=1}^{n} \dot{q}_j^{b_j} \prod_{l=1}^{m} q_{\mathrm{se},l}^{e_l} \prod_{j=1}^{n} Z_j^{f_j} \cdot \dot{q}_{r-n}^{-1} g_r\right] \\ &+ \sum_{r=2n+1}^{2n+m} e_{r-2n} \mathbb{E}\left[\prod_{j=1}^{n} q_j^{a_j} \prod_{j=1}^{n} \dot{q}_j^{b_j} \prod_{l=1}^{m} q_{\mathrm{se},l}^{e_l} \prod_{j=1}^{n} Z_j^{f_j} \cdot q_{\mathrm{se},r-2n}^{-1} g_r\right] \\ &+ \sum_{r=2n+m+1}^{3n+m} f_{r-2n-m} \mathbb{E}\left[\prod_{j=1}^{n} q_j^{a_j} \prod_{j=1}^{n} \dot{q}_j^{b_j} \prod_{l=1}^{m} q_{\mathrm{se},l}^{e_l} \prod_{j=1}^{n} Z_j^{f_j} \cdot Z_{r-2n-m}^{-1} g_r\right] \\ &+ \frac{1}{2} \sum_{r=2n+m+1, s=2n+m+1, r\neq s}^{3n+m,3n+m} f_{r-2n-m} f_{s-2n-m} \left(\boldsymbol{h}\boldsymbol{h}^T\right)_{rs} \\ &\mathbb{E}\left[\prod_{j=1}^{n} q_j^{a_j} \prod_{j=1}^{n} \dot{q}_j^{b_j} \prod_{l=1}^{m} q_{\mathrm{se},l}^{e_l} \prod_{j=1}^{n} Z_j^{f_j} \cdot Z_{r-2n-m}^{-1} Z_{s-2n-m}^{-1}\right] \\ &+ \frac{1}{2} \sum_{r=2n+m+1}^{3n+m,} f_{r-2n-m}(f_{r-2n-m} - 1) \left(\boldsymbol{h}\boldsymbol{h}^T\right)_{rr} \\ &\mathbb{E}\left[\prod_{j=1}^{n} q_j^{a_j} \prod_{j=1}^{n} \dot{q}_j^{b_j} \prod_{l=1}^{m} q_{\mathrm{se},l}^{e_l} \prod_{j=1}^{n} Z_j^{f_j} \cdot Z_{r-2n-m}^{-2}\right]\end{aligned} \tag{22}$$

The above formula is named as state augmentation method in [27]. It is should be noted that $\mathbb{E}\left[\frac{\partial m(\,)}{\partial t}\right] = 0$, when the moments function $m(\,)$ does not depend explicitly on time t, and transient part depending on the initial conditions is ignored. Also, $\frac{d\mathbb{E}[m(\,)]}{dt} = 0$ when $t \to \infty$ and $\boldsymbol{Z}(t)$ are stationary processes.

3. Numerical application

3.1. Description of analyzed bridges

In this study, a simulated long-span bridge with a main span of 1263 m and deck width of 27.43 m is employed to examine the non-Gaussian turbulence effect on the bridge buffeting vibration. The key geometry parameters of the bridge are illustrated in Fig. 2. The main structural and aerodynamic parameters are shown in Table 1.

For simplicity and without loss of generality, only the first vertical and torsional modes of the examined bridge [39] are considered in this study (n = 2). The first vertical mode and torsional mode frequencies are 0.0870, 0.1916 Hz, respectively, and both corresponding mode shapes are sinusoidal anti-symmetric.

Theodorsen function is used to evaluate the values of eight flutter derivatives H_1^* - H_4^* and A_1^* - A_4^* [40]; other flutter derivatives are not considered in this study, but can be derived based on quasi-steady theory or determined by 3 directional sectional model wind tunnel test if necessary. $\chi_{L_{\mathrm{bu}}}$, $\chi_{L_{\mathrm{bw}}}$, $\chi_{M_{\mathrm{bu}}}$ and $\chi_{M_{\mathrm{bw}}}$ are approximated by Sears function [41].

In the turbulence simulation, von Kármán and Panofsky type spectrum are used for the along-wind and vertical turbulence spectra, respectively. The along-wind and vertical turbulence intensity I_u and I_w are both assumed as 0.1, and the turbulence integral length L_u and L_w is dependent on intensity as the relationship presented in [29]. The turbulence coherence decay coefficients C_u and C_w in Eq. (12).

3.2. Moments function for bridge buffeting response

In order to simplify the computational effects in this example, there are several assumptions listed below:

- The aerodynamic memory effect is ignored. Therefore, memory effect expansion order m in Eq. (4) is 0, and $\boldsymbol{q}_{se}$ is vanished. However, if the aerodynamic memory effect is required, $\boldsymbol{q}_{se}$ can be included in the buffeting response evaluation procedure by increasing the dimension of $\boldsymbol{g}(\boldsymbol{X}(t), t)$ in Eq. (18).
- Only the first vertical and torsional modes of the analyzed bridges are employed in this study, which is common practice for bridge buffeting response [39,42]. Therefore, modes number n in Eq. (22) is 2. For large span bridges, when modal frequencies are closely spaced, more modes should be considered into the dynamic system. For streamlined sectional shape used by long-span bridges, the along-wind responses p for bridge girders induced by drag forces D have been of less concern because of insignificant drag coefficient and the high width-to-depth ratio.
- The aerodynamic mass A_3 is ignored because the wind speed in the atmospheric boundary layer is far below the speed of sound [43]. Thus, $\bar{\boldsymbol{M}}$ in Eq. (16) is an identity matrix with degree of m.
- The transfer function from turbulence to buffeting force (aerodynamic admittance) is linear, and the skewness and kurtosis of buffeting force are equal to skewness and kurtosis of turbulence. The proof is presented in Appendix.

Applying the above assumption on the steady-state equation in Eq. (16), the element-by-element matrix equation is

$$d\begin{bmatrix} q_1 \\ q_2 \\ \dot{q}_1 \\ \dot{q}_2 \\ Z_1 \\ Z_2 \end{bmatrix}$$

$$= \begin{bmatrix} 0 & 0 & 1 & 0 & 0 & 0 \\ 0 & 0 & 0 & 1 & 0 & 0 \\ -k_{11} & -k_{12} & -c_{11} & -c_{12} & \sum_{k=0}^{K} g_{k,1} Z_1^{k-1}(t) & 0 \\ -k_{21} & -k_{22} & -c_{21} & -c_{22} & 0 & \sum_{k=0}^{K} g_{k,2} Z_2^{k-1}(t) \\ 0 & 0 & 0 & 0 & -\alpha_{11} & -\alpha_{12} \\ 0 & 0 & 0 & 0 & -\alpha_{21} & -\alpha_{22} \end{bmatrix}$$

$$\times \begin{bmatrix} q_1 \\ q_2 \\ \dot{q}_1 \\ \dot{q}_2 \\ Z_1 \\ Z_2 \end{bmatrix} dt + \begin{bmatrix} 0 & 0 \\ 0 & 0 \\ 0 & 0 \\ 0 & 0 \\ \Theta_{11} & \Theta_{12} \\ \Theta_{21} & \Theta_{22} \end{bmatrix} \begin{bmatrix} dW_1(t) \\ dW_2(t) \end{bmatrix} \tag{23}$$

with state vector as
$\boldsymbol{X} = \begin{bmatrix} \boldsymbol{q} & \dot{\boldsymbol{q}} & \boldsymbol{Z} \end{bmatrix}^T = \begin{bmatrix} q_1 & q_2 & \dot{q}_1 & \dot{q}_2 & Z_1 & Z_2 \end{bmatrix}^T$.

The standardized Itô equation of above equation is

$$d \begin{bmatrix} q_1 \\ q_2 \\ \dot{q}_1 \\ \dot{q}_2 \\ Z_1 \\ Z_2 \end{bmatrix} = \begin{bmatrix} \dot{q}_1 \\ \dot{q}_2 \\ -k_{11}q_1 - k_{12}q_2 - c_{11}\dot{q}_1 - c_{12}\dot{q}_2 + \sum_{k=0}^{K} g_{k,1} Z_1^k(t) \\ -k_{21}q_1 - k_{22}q_2 - c_{21}\dot{q}_1 - c_{22}\dot{q}_2 + \sum_{k=0}^{K} g_{k,2} Z_2^k(t) \\ -\alpha_{11} Z_1(t) - \alpha_{12} Z_2(t) \\ -\alpha_{21} Z_1(t) - \alpha_{22} Z_2(t) \end{bmatrix} dt$$

$$+ \begin{bmatrix} 0 & 0 \\ 0 & 0 \\ 0 & 0 \\ 0 & 0 \\ \Theta_{11} & \Theta_{12} \\ \Theta_{21} & \Theta_{22} \end{bmatrix} \begin{bmatrix} dW_1(t) \\ dW_2(t) \end{bmatrix} \tag{24}$$

Substituting the above equation into Eq. (22), the system of linear equations for the bridge motion with aeroelasticity became as

$$\begin{aligned} 0 = & -(b_1 c_{11} + b_2 c_{22} + f_1 \alpha_{11} + f_2 \alpha_{22}) m(a_1, a_2, b_1, b_2, f_1, f_2) \\ & + a_1 m(a_1 - 1, a_2, b_1 + 1, b_2, f_1, f_2) + a_2 m(a_1, a_2 - 1, b_1, b_2 + 1, f_1, f_2) \\ & - b_1 k_{11} m(a_1 + 1, a_2, b_1 - 1, b_2, f_1, f_2) \\ & - b_1 k_{12} m(a_1, a_2 + 1, b_1 - 1, b_2, f_1, f_2) \\ & - b_2 k_{21} m(a_1 + 1, a_2, b_1, b_2 - 1, f_1, f_2) \\ & - b_2 k_{22} m(a_1, a_2 + 1, b_1, b_2 - 1, f_1, f_2) \\ & - b_1 c_{12} m(a_1, a_2, b_1 - 1, b_2 + 1, f_1, f_2) \\ & - b_2 c_{21} m(a_1, a_2, b_1 + 1, b_2 - 1, f_1, f_2) \\ & + b_1 \sum_{k=0}^{K} g_{k,1} m(a_1, a_2, b_1 - 1, b_2, f_1 + k, f_2) \\ & + b_2 \sum_{k=0}^{K} g_{k,2} m(a_1, a_2, b_1, b_2 - 1, f_1, f_2 + k) \\ & - f_1 \alpha_{12} m(a_1, a_2, b_1, b_2, f_1 - 1, f_2 + 1) \\ & - f_2 \alpha_{21} m(a_1, a_2, b_1, b_2, f_1 + 1, f_2 - 1) \\ & + f_1 f_2 \left(\Theta_{11}\Theta_{21} + \Theta_{12}\Theta_{22}\right) m(a_1, a_2, b_1, b_2, f_1 - 1, f_2 - 1) \\ & + \frac{1}{2} f_1 (f_1 - 1) \left(\Theta_{11}^2 + \Theta_{12}^2\right) m(a_1, a_2, b_1, b_2, f_1 - 2, f_2) \\ & + \frac{1}{2} f_2 (f_2 - 1) \left(\Theta_{21}^2 + \Theta_{22}^2\right) m(a_1, a_2, b_1, b_2, f_1, f_2 - 2) \end{aligned} \tag{25}$$

Similar to the state augmentation method with single DOF in [26], The moments of order $\mathbb{s} = a_1 + a_2 + b_1 + b_2$ can be obtained from Eq. (25) through subsequently increasing $a_1+a_2+b_1+b_2$ from 1 to $\mathbb{s}$. For any value of $\mathbb{s}$, a total number of $\binom{\mathbb{s}+3}{\mathbb{s}} = \frac{(\mathbb{s}+3)!}{\mathbb{s}!3!}$ linear equations can be established by Eq. (25). Before determining the moments function $m(a_1, a_2, b_1, b_2, f_1, f_2)$ before order $\mathbb{s}$, the calculation of moments $m(a_1, a_2, b_1, b_2, f_1, f_2)$ for $a_1 + a_2 + b_1 + b_2 = 0$, $f_1 + f_2 = 0, 1, 2, \ldots, (\mathbb{s})K$; $a_1 + a_2 + b_1 + b_2 = 1$, $f_1 + f_2 = 0, 1, 2, \ldots, (\mathbb{s}-1)K$; $a_1 + a_2 + b_1 + b_2 = 2$, $f_1+f_2 = 1, 2, \ldots, (\mathbb{s}-2)K$ until $a_1+a_2+b_1+b_2 = \mathbb{s}-1$, $f_1+f_2 = 0, 1, 2, \ldots, K$ are required.

For the initial case with $a_1 + a_2 + b_1 + b_2 = 1$, $m(a_1, a_2, b_1, b_2, f_1, f_2)$ can be calculated recursively for increasing values of $f_1 + f_2$. For $a_1+a_2+b_1+b_2 = 0$, $m(0, 0, 0, 0, f_1, f_2)$ can be found according to Isserlis' theorem in [44]

$$m(0,0,0,0,f_1,f_2) = \begin{cases} 0 \\ \text{if } f_1 + f_2 \text{ is odd,} \\ \sigma_{11}^{f1} \sigma_{22}^{f2} \dfrac{f_1! f_2!}{2^{(f_1+f_2)/2}} \displaystyle\sum_{v=0}^{\min[f_1,f_2]/2} \\ \times \dfrac{(2\frac{\sigma_{12}}{\sqrt{\sigma_{11}\sigma_{22}}})^{2v}}{\left(\frac{f_1}{2} - v\right)! \left(\frac{f_2}{2} - v\right)! (2v)!} \\ \text{if } f_1 \text{ and } f_2 \text{ are even,} \\ \sigma_{11}^{f1} \sigma_{22}^{f2} \dfrac{f_1! f_2!}{2^{(f_1+f_2)/2}} \displaystyle\sum_{v=0}^{\min[f_1,f_2]/2} \\ \times \dfrac{(2\frac{\sigma_{12}}{\sqrt{\sigma_{11}\sigma_{22}}})^{2v+1}}{\left(\frac{f_1 - 1}{2} - v\right)! \left(\frac{f_2 - 1}{2} - v\right)! (2v+1)!} \\ \text{if } f_1 \text{ and } f_2 \text{ are odd.} \end{cases} \tag{26}$$

3.3. Verification of fitting buffeting force by Ornstein–Uhlenbeck process

The PSD matrix of bridge buffeting forces can be calculated by Eq. (11). When the turbulence is non-Gaussian, and its non-negligible skewness and kurtosis will be directly transferred to buffeting force with the assumption that vertical and along-wind turbulences have the same skewness and kurtosis.

The corresponding standardized Gaussian process $\tilde{\boldsymbol{Z}}$ can be derived according to the spectrum distortion method [30] with PSD denoted as $S_{\tilde{Z}\tilde{Z}}$. In this study, the multivariate Ornstein–Uhlenbeck (OU) processes $\boldsymbol{Z}(t; \boldsymbol{\alpha}, \boldsymbol{\Theta})$ defined in Eq. (14) is employed to fit the underlying buffeting forces $\tilde{\boldsymbol{Z}}$.

The PSD of multivariate OU processes is

$$S_{ZZ}(\omega) = (-\imath\omega \boldsymbol{I} + \boldsymbol{\alpha})^{-1} \left(\boldsymbol{\alpha}\mathbb{K} + \mathbb{K}\boldsymbol{\alpha}^T\right) \left(\imath\omega \boldsymbol{I} + \boldsymbol{\alpha}^T\right)^{-1} \tag{27}$$

The relationship among $\boldsymbol{\alpha}$, $\boldsymbol{\Theta}$ and $\mathbb{K}$ is defined in Eq. (15). After all, through fitting $\boldsymbol{\alpha}$ and $\boldsymbol{\Theta}$, the underlying buffeting forces $\tilde{\boldsymbol{Z}}$ can be approximated by OU processes $\boldsymbol{Z}(t; \boldsymbol{\alpha}, \boldsymbol{\Theta})$.

When wind speeds $U = 40$ m/s, $I_u = I_w = 0.1$, $L_u = 76.4$ m and $L_w = 16.9$ m, the PSD of transformed bridge buffeting forces according to Eqs. (11) and (13) including 1st vertical (noted as 1) and torsional mode (noted as 2) are plotted in Fig. 3. Fig. 3a is the PSD for lift force, Fig. 3b is the PSD for pitch moment and Fig. 3c is the cross PSD between lift force and pitch moment. The buffeting force covariance $\mathbb{K}$ can be found through integrating PSD $S_{ZZ}(\omega)$ from $\omega = 0$ to $\omega = \infty$. The values of $\boldsymbol{\alpha}$ and $\boldsymbol{\Theta}$ can be determined through minimizing the difference between $S_{\tilde{Z}\tilde{Z}}$ and S_{ZZ} using gradient descent optimization algorithms.

The comparison between $S_{\tilde{Z}\tilde{Z}}$ and S_{ZZ} shows that OU process is able to approximate the buffeting forces random process with sufficient accuracy.

3.4. Verification of buffeting responses calculated by state augmentation method

When the turbulence u and w are Gaussian process, the buffeting force random process $\boldsymbol{Q}_{\mathrm{b}}(t)$ will be reduced as:

$$\boldsymbol{Q}_{\mathrm{b}}(t) = \mathbf{g}_1 \tilde{\boldsymbol{Z}}(t). \tag{28}$$

Thus, the structural buffeting response can be calculated by the state augmentation method in Eq. (25) with $\mathbb{s} = 2$. Because the

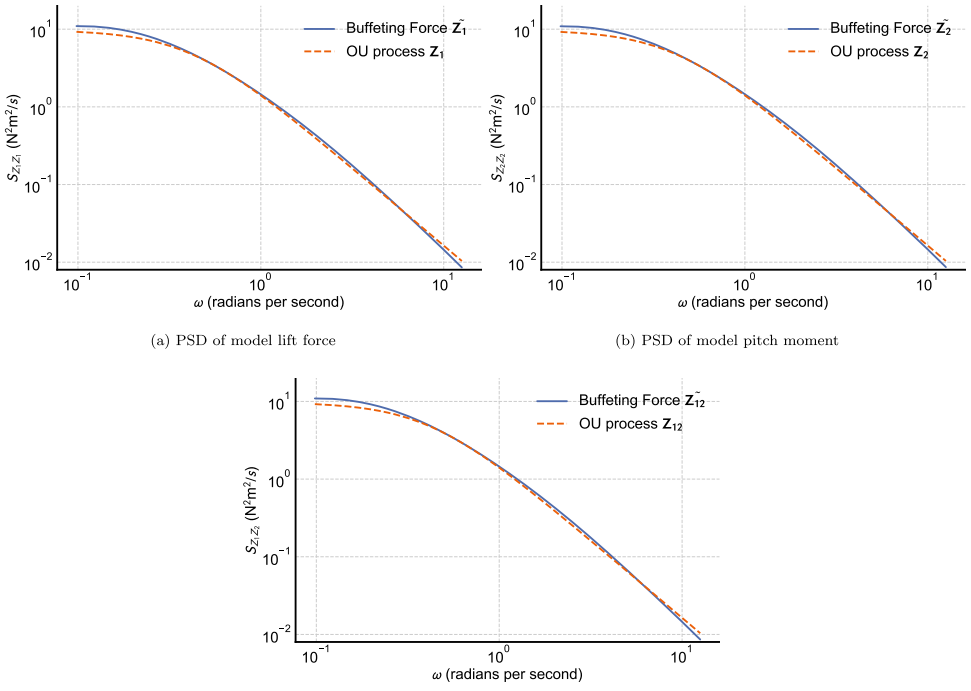

(a) PSD of model lift force

(b) PSD of model pitch moment

(c) Cross PSD between Lift and Torque

Fig. 3. PSD Comparison between fitted OU process and underlying buffeting forces.

structural random excitation is Gaussian, the buffeting responses will be Gaussian as well. In other words, because the structural system is linear and complete, the moments function $m(a_1, a_2, b_1, b_2, 0, 0) = 0$ for $a_1 + a_2 + b_1 + b_2 > 2$ [45]. The RMS value of bridge vertical and torsional response can be determined from the moments function $m(a_1 = 2, 0, 0, 0, 0, 0)$ and $m(0, 0, b_1 = 2, 0, 0, 0)$ according to the procedure described in Section 3.2.

In order to validate the accuracy of the state augmentation method used in this study, the RMS value of structural buffeting response can be derived from classical frequency domain analysis method [3,46]. The results comparison between frequency domain analysis and state augmentation method are presented in Fig. 4.

Fig. 4 shows that the buffeting responses calculated by state augmentation method have an accuracy close to the frequency domain method. However, the small differences from state augmentation do exist because of buffeting force expressed by OU process slightly deviates from the original buffeting force shown in Fig. 3.

4. Buffeting responses induced by non-Gaussian turbulence

After the state augmentation method has been verified for both buffeting responses and Gaussian turbulence induced vibration at the above section, the buffeting responses induced by non-Gaussian turbulence will be studied in this section. The non-Gaussian turbulence will be approximated by summation of 4th order Hermite polynomials, which means $K = 4$ in Eqs. (13) and (25). Expanding the state augmentation order $\mathbb{s}$ to 4, the state augmentation formula in Eq. (25) can be employed to calculate up to the 4th order moments of structural response, such as $m(3, 0, 0, 0, 0, 0)$ and $m(4, 0, 0, 0, 0, 0)$ which means 3rd and 4th moments of structural vertical responses.

4.1. RMS buffeting responses

In this case study, the wind speeds U range is [20–60] m/s with 5 m/s as step gap, and the skewness $\gamma_{u,w}$ is [0, 2] with 0.2 as step gap. The turbulence kurtosis is considered as depending solely on skewness [29]. The RMS vertical and torsional responses for a different

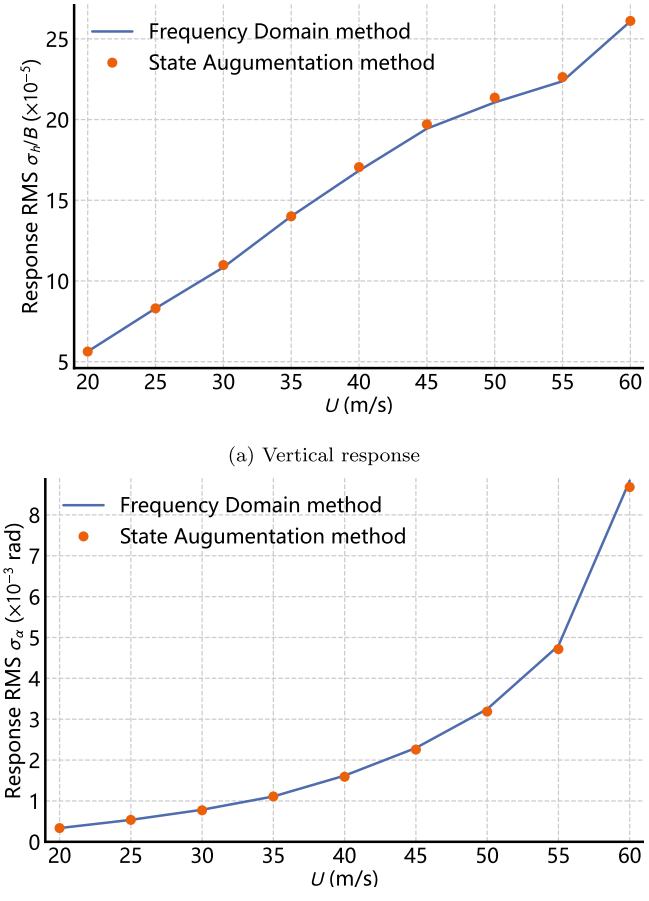

(a) Vertical response

(b) Torsional response

Fig. 4. Comparison of RMS buffeting response calculated by frequency domain analysis and state augmentation method.

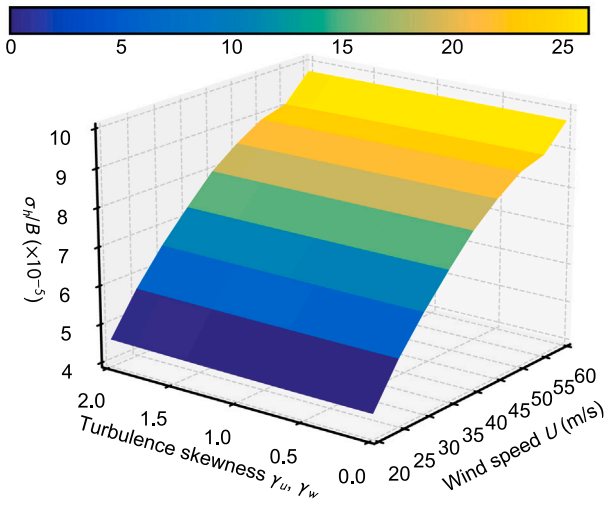

(a) Vertical response

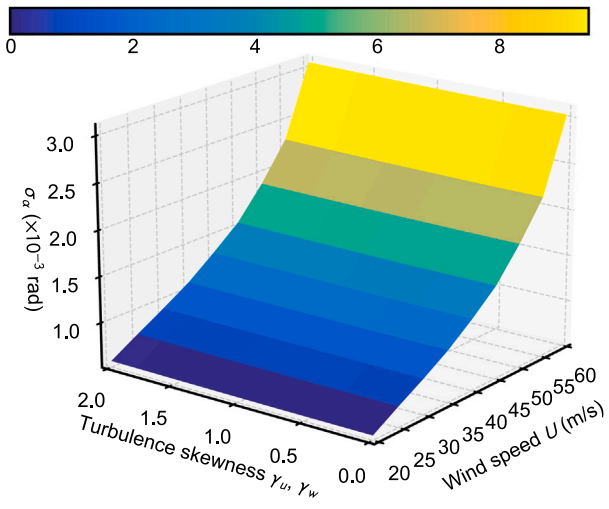

(b) Torsional response

Fig. 5. RMS buffeting vibration caused by non-Gaussian turbulence.

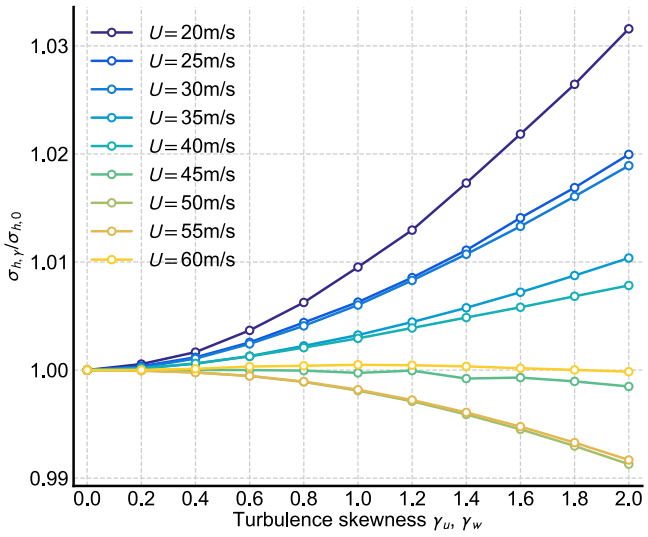

(a) Vertical response

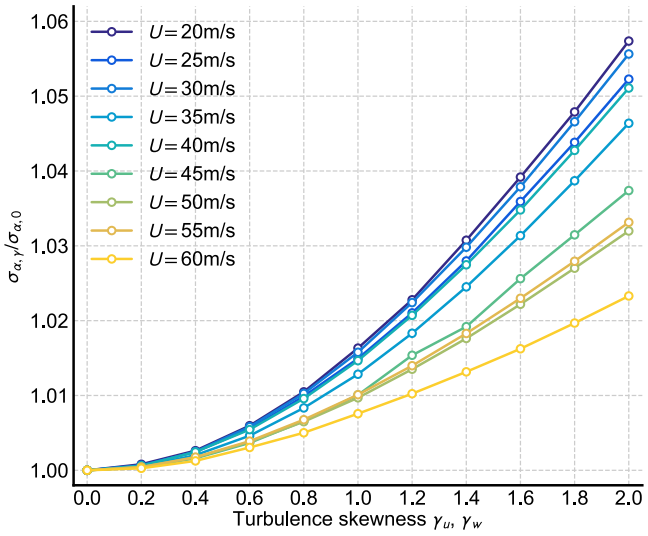

(b) Torsional response

Fig. 6. Turbulence skewness affected buffeting response normalized by Gaussian turbulence induced response.

combination of wind speeds and turbulence skewness are plotted in Figs. 5a and 5b, respectively. The results show that wind speed is the dominating factor rather than turbulence skewness $\gamma_{u,w}$. The increasing trend of vertical response σ_h becomes slower for higher wind speeds because of the increased vertical aerodynamic damping, while the increasing trends of torsional response become higher for decreased torsional damping. When wind speed is $U = 60$ m/s, both vertical and torsional response increasing dramatically since wind speed is close to the critical flutter speed.

In order to emphasize the turbulence skewness effect on the bridge buffeting response, the buffeting RMS response $\sigma_{h,\gamma}$ and $\sigma_{\alpha,\gamma}$ are normalized to the vibration amplitudes from Gaussian turbulence $\gamma = 0$ for each different wind speeds, and the results are plotted in Figs. 6a and 6b, respectively. For both vertical and torsional responses, turbulence skewness has a small effect on the RMS responses. As the wind speeds increase, the increasing ratio for turbulence skewness is reduced because of the aerodynamic damping and aerodynamic stiffness. Especially for vertical response with higher wind speeds $U \geq 45$ m/s, the turbulence skewness has a negative effect on buffeting responses. However, generally speaking, the effect from turbulence skewness on buffeting responses is insignificant for long-span bridges.

4.2. Skewness and kurtosis of buffeting response

Besides the RMS buffetings responses, another concern is whether the non-Gaussianity of turbulence will be transferred to the non-Gaussianity of responses. Thus, the structural response skewness and excessive kurtosis (kurtosis for simplicity in the remaining text.), which are defined in Eq. (29), can be calculated based on Eq. (25) when the state augmentation order $\mathbb{s}$ is 4.

$$\gamma_h = \frac{m(3,0,0,0,0,0)}{m(2,0,0,0,0,0)^{3/2}} \tag{29a}$$

$$\kappa_h = \frac{m(4,0,0,0,0,0)}{m(2,0,0,0,0,0)^{4/2}} - 3 \tag{29b}$$

$$\gamma_\alpha = \frac{m(0,0,3,0,0,0)}{m(0,0,2,0,0,0)^{3/2}} \tag{29c}$$

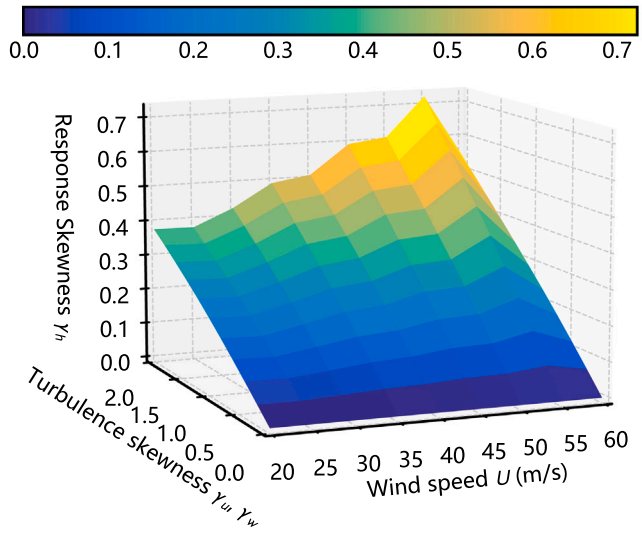

(a) Vertical response

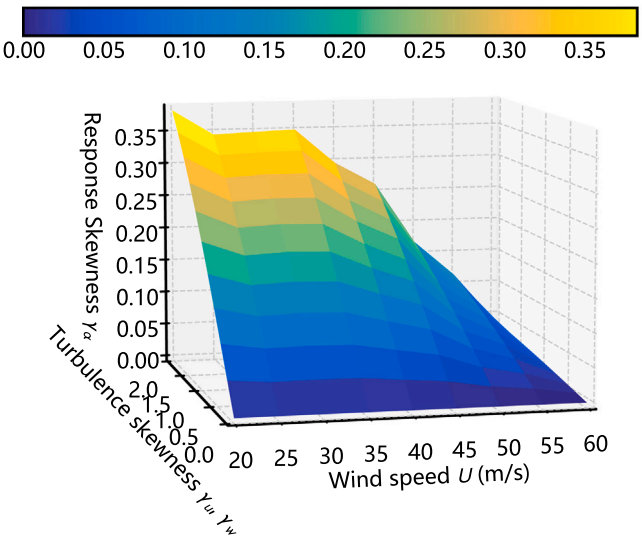

(b) Torsional response

Fig. 7. Skewness of buffeting response affected by turbulence skewness.

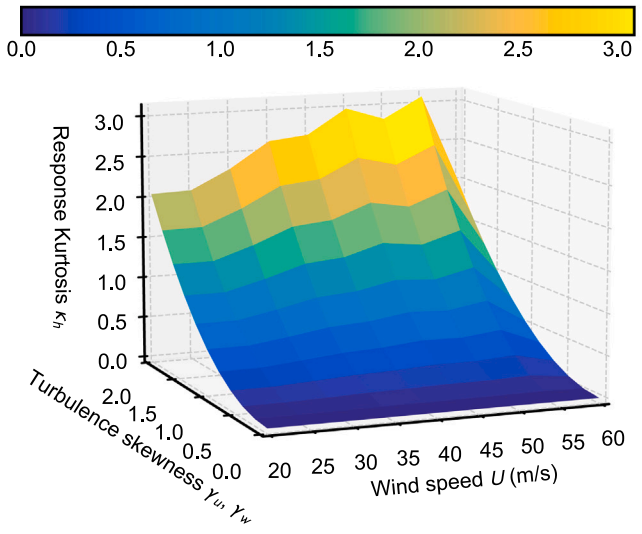

(a) Vertical response

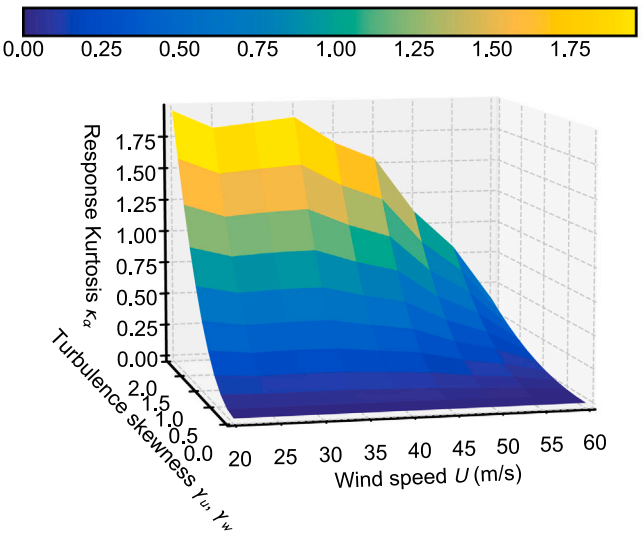

(b) Torsional response

Fig. 8. Kurtosis of buffeting response affected by turbulence skewness.

$$\kappa_\alpha = \frac{m(0,0,4,0,0,0)}{m(0,0,2,0,0,0)^{4/2}} - 3 \tag{29d}$$

The buffeting responses skewness and kurtosis of long-span bridge are plotted in Figs. 7 and 8, respectively. For second-order differential equations without damping, the system response will be sinusoidal regardless of the type of external forces. Therefore, for long-span bridge buffeting response, the response should be Gaussian excited by either Gaussian or non-Gaussian turbulence. Even for a slightly damped system (the damping is smaller than 5‰), the structural response is also close to Gaussian. However, for long-span bridges, the deck motion-induced aerodynamic damping and aerodynamic stiffness will make the structural response more complex. For vertical response, as the wind speeds increase, the skewness of buffeting vibration γ_h also becomes larger because of increasing aerodynamic damping. The only exception is $U = 60$ m/s, because at this wind speed, the bridge is close to flutter and the strong coupling between vertical and torsional motion. In contrast, for the torsional response, the skewness of buffeting vibration γ_α becomes smaller because of decreased aerodynamic damping.

The response kurtosis κ_h and κ_α have similar trending as the skewness, which indicates that the kurtosis has a strong correlation with skewness. Overall, even though the RMS response is slightly affected by turbulence skewness, the response skewness and kurtosis are worth to be investigated. Furthermore, because the distribution of the response is affected by skewness and kurtosis, its extreme responses will also be affected, which will be studied in the next section.

4.3. Extreme vibration caused by non-Gaussian turbulence

When the bridge vibration caused by non-Gaussian turbulence also contains non-negligible skewness and kurtosis, the probability distribution function (PDF) will also deviate from the normal distribution. When skewness is positive, as in Fig. 7, the tail along the positive direction is thicker than the normal distribution. Therefore, the extreme response from skewed distribution will be larger than the extreme response from Gaussian response even their standard deviations are

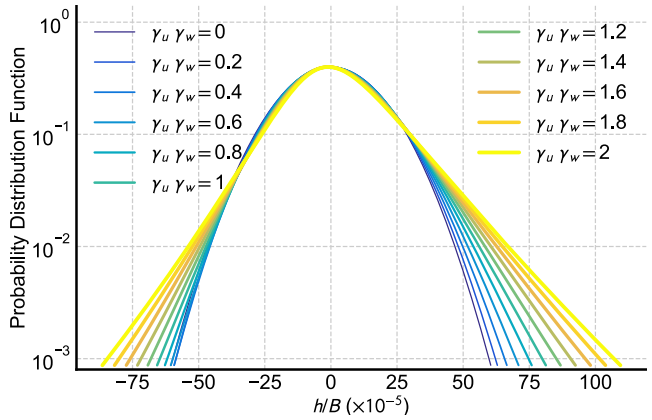

Fig. 9. Probability distribution function of vertical response subjected to non-Gaussian turbulence with different skewness when $U = 40$ m/s.

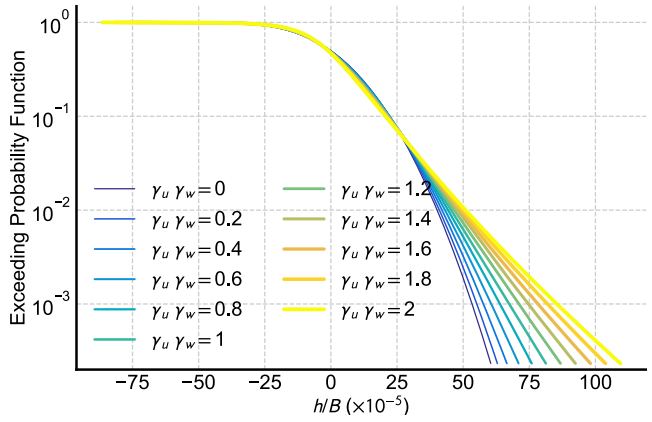

Fig. 10. Exceeding probability function of vertical response subjected to non-Gaussian turbulence with different skewness when $U = 40$ m/s.

only slightly affected by non-Gaussian turbulence. Gram–Charlier expansion [47] is employed to approximate the PDF of structural response from the calculated moments. Fig. 9 plots the PDF of bridge vertical response when $U = 40$ m/s affected by non-Gaussian turbulence with different skewness from 0 to 2. It clearly shows that the response PDFs are skewed towards positive direction, and the PSD tails also become thicker for vibration caused by non-Gaussian turbulence with larger turbulence.

Fig. 10 plot the exceeding probability function (1 - cumulative probability function) of vertical bridge response when $U = 40$ m/s, which clearly shows the tail shape is affected by non-Gaussian turbulence. For the same exceeding probability, the corresponding vibration caused by non-Gaussian turbulence with larger skewness will be much larger than the vibration caused by Gaussian turbulence. In the following, the extreme responses calculated from the up-crossing formula are compared among turbulence with different skewness.

4.3.1. Extreme buffeting response based on up-crossing theory

For Gaussian random responses, the extreme response is normally expressed by multiplication of RMS response by a peak factor. For example, the extreme vertical response is calculated as:

$$h_{\max} = g_h \sigma_h \tag{30}$$

in which $h_{\max}$ is the vertical extreme response and g_h is vertical peak factor. The peak factor can be estimated from famous Rice's formula [48].

$$g_h = \beta_h + \frac{\gamma_e}{\beta_h} \tag{31}$$

in which $\beta_h = \sqrt{2\ln(\nu_{0,h}T)}$, $\nu_{0,h} = \dfrac{\sigma_{\dot{h}}}{\sigma_h}$, γ_e is Euler's constant (0.5772) and T is the observation duration, which is normally 600 s. $\sigma_{\dot{h}}$ is the RMS vertical moving velocity, which equal to $\sqrt{m(0,2,0,0,0,0)}$.

When a long-span bridge is excited by non-Gaussian turbulence, the buffeting response contains non-Gaussian characteristics too. Similar to non-Gaussian turbulence, it can be approximated as a memory-less function of an underlying standard Gaussian process $v(t)$:

$$h(t) = g_h(v(t)) = \mathbb{k}\left[v(t) + \mathbb{h}_3(v^2(t)-1) + \mathbb{h}_4(v^3(t)-3v(t))\right] \tag{32a}$$

$$\mathbb{h}_3 = \frac{\gamma_h}{4 + 2\sqrt{1+1.5\kappa_h}} \tag{32b}$$

$$\mathbb{h}_4 = \frac{\sqrt{1+1.5\kappa_h}-1}{18} \tag{32c}$$

$$\mathbb{k} = \frac{1}{\sqrt{1+2\mathbb{h}_3^2+6\mathbb{h}_4^2}} \tag{32d}$$

in which $\mathbb{h}_3$, $\mathbb{h}_4$ and $\mathbb{k}$ are Hermite polynomial coefficients of process $h(t)$.

According to the formula of peak factors of non-Gaussian process [49]:

$$g_{\mathrm{ng},h} = \mathbb{k}\left\{\left(\beta_h + \frac{\gamma_e}{\beta_h}\right) + \mathbb{h}_3\left[\beta_h^2 + (2\gamma_e - 1) + \frac{1.98}{\beta_h^2}\right] + \mathbb{h}_4\left[\beta_h^3 + 3\beta_h(\gamma_e - 1) + \frac{3}{\beta_h}\left(\frac{\pi^2}{6} - \gamma_e + \gamma_e^2\right) + \frac{5.44}{\beta_h^3}\right]\right\}. \tag{33}$$

In the above two formulas, the second, third, and fourth moments of vertical response $h(t)$, as well as the second moment of vertical moving velocity $\dot{h}(t)$ can be found using state augmentation method in Eq. (22).

4.3.2. Results of extreme responses

According to Eq. (33) and long-span bridges buffeting response RMS value, skewness, kurtosis response in the previous section, the peak factors for various combinations of wind speeds and turbulence skewness are plotted in Figs. 11a and 11b for the vertical and torsional response, respectively. The peak factors for non-Gaussian turbulence-induced vibration are larger than vibration caused by Gaussian turbulences. The overall changing trending is similar to response skewness and kurtosis. After the calculation of peak factors, the extreme response for both vertical and torsional will be determined by Eq. (30). Similar to RMS response comparisons in Fig. 6, the peak buffeting responses induced by non-Gaussian turbulence are normalized to corresponding responses caused by Gaussian turbulence as in Fig. 12. In contrast with RMS response, the effect of turbulence skewness on peak response is much more significant because of responses skewness and kurtosis. For the torsional responses, the effect of turbulence skewness decreases rapidly for larger wind speeds. Differently, for the vertical responses, the increment ratio due to turbulence skewness is more stable. In summary, the long-span buffeting vibration caused by non-Gaussian turbulence has larger vibrations extremes, which cannot be ignored when wind turbulence has non-Gaussian features.

5. Conclusions

This paper firstly introduced the long-span bridge buffeting caused by turbulent winds and described the existence of non-Gaussian turbulence. Then, a method has been derived for calculating the bridge buffeting response statistics based on the state augmentation method. This method involved five steps. First, the PSD of buffeting forces are calculated from non-Gaussian turbulence, and Hermite polynomials are determined by the associated skewness and kurtosis. Second, the multivariate Ornstein–Uhlenbeck process is used to proximate the random buffeting forces time sequence. Third, the state augmentation formula is established for long-span bridge buffeting, considering the aerodynamic

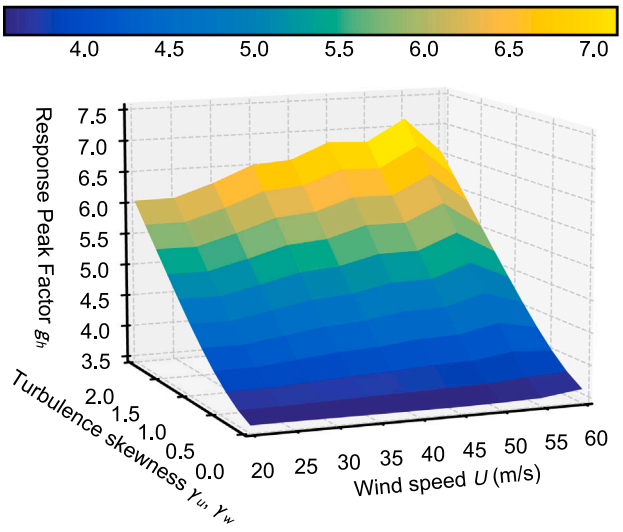

(a) Vertical response

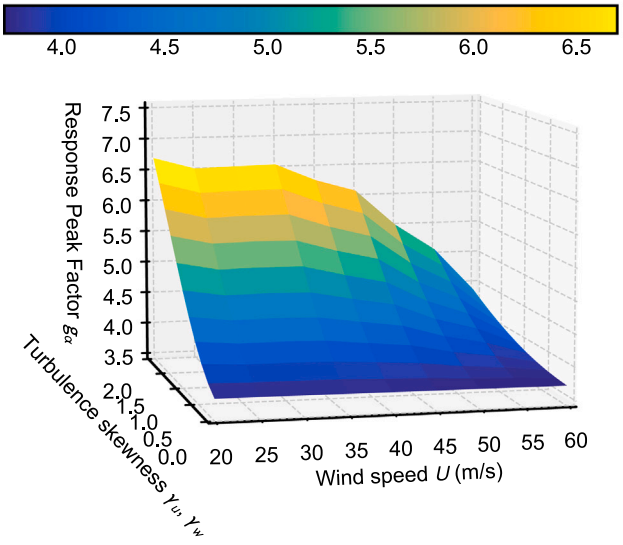

(b) Torsional response

Fig. 11. Peak factors of buffeting response affected by turbulence skewness.

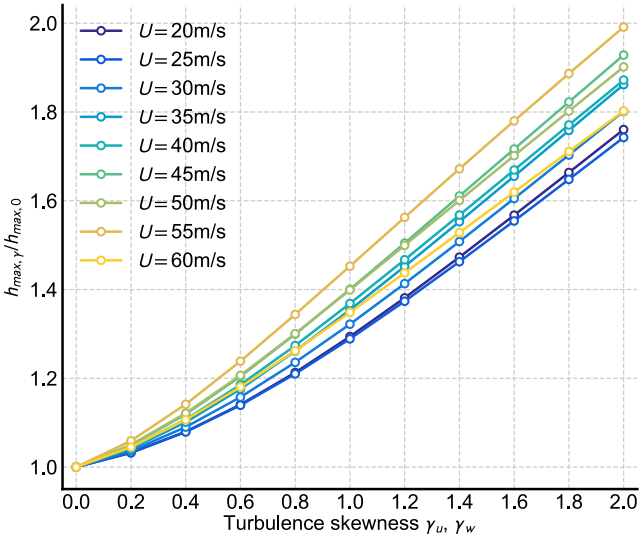

(a) Vertical response

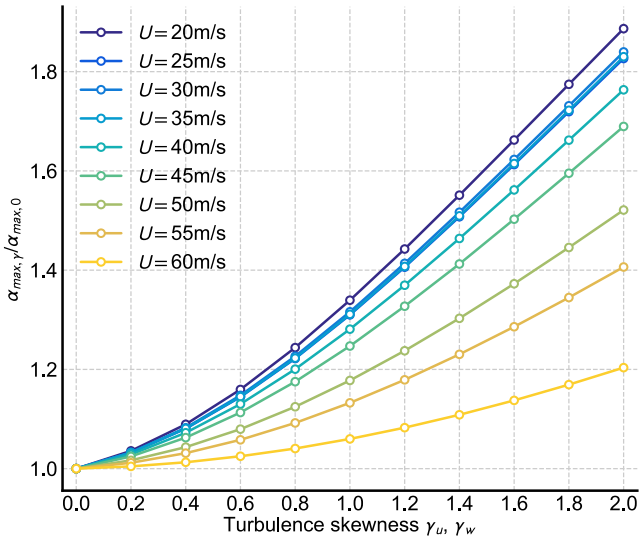

(b) Torsional response

Fig. 12. Turbulence skewness affected extreme buffeting response normalized by Gaussian turbulence induced response extremes.

coupling between vertical and torsional responses. Fourth, the moments of bridge vertical and torsional response can be calculated from 2nd to 4th order sequentially, and the corresponding response RMS, skewness, and kurtosis are computed. Fifth, the extreme response is derived from the peak factor considering the responses skewness and kurtosis.

Results show that when the long-span bridge is excited by non-Gaussian turbulence, the responses RMS values are slightly affected. The increment ratio increased with larger wind speeds for vertical responses but decreased for torsional responses because of the aerodynamic damping related to flutter derivatives. On the other side, peak factors are also affected by responses skewness and kurtosis. Therefore, the extreme responses increase substantially comparing with Gaussian turbulence-induced vibrations. Nevertheless, it should be noted that the buffeting force approximated by OU process should be close at the structural resonant frequency, otherwise the results from proposed state augment formula will be inaccurate. Also, the analytical formula derived in this study only involve two modes, which should be expanded to more modes, especially for long-span bridges. Furthermore, the turbulence to aerodynamic force conversion under non-Gaussian turbulence should be investigated experimental or analytically to provide more an accurate approximation of non-Gaussian turbulence induced vibration.

CRediT authorship contribution statement

Wei Cui: Writing – original draft, Conceptualization, Formal analysis, Investigation, Methodology, Validation, Visualization. **Lin Zhao:** Supervision, Writing – review & editing, Funding acquisition. **Yaojun Ge:** Supervision, Funding acquisition.

Declaration of competing interest

The authors declare that they have no known competing financial interests or personal relationships that could have appeared to influence the work reported in this paper.

Acknowledgments

The authors gratefully acknowledge the support of National Natural Science Foundation of China (52008314, 52078383) and Shanghai Pujiang Program, China (No. 19PJ1409800). Any opinions, findings and conclusions or recommendations are those of the authors and do not necessarily reflect the views of the above agencies.

Appendix. Transfer of skewness and kurtosis from non-gaussian turbulence to buffeting force

Let u be a non-Gaussian turbulence with skewness as γ_u and kurtosis as κ_u, and the expectation of u is $\mathbb{E}[u] = 0$.

Let the transfer function from turbulence to buffeting force $L = \mathbb{L}(u)$ and the $\mathbb{L}$ is an arbitrary linear function with 0 interceptions, such as $L = a \times u$.

Thus the skewness of buffeting force can be found as

$$\gamma_L = \frac{\mathbb{E}[L^3]}{\mathbb{E}[L^2]^{3/2}} = \frac{\mathbb{E}[\mathbb{L}(u)^3]}{\mathbb{E}[\mathbb{L}(u)^2]^{3/2}} = \frac{\mathbb{E}[a^3u^3]}{\mathbb{E}[a^2u^2]^{3/2}} = \frac{\mathbb{E}[u^3]}{\mathbb{E}[u^2]^{3/2}} = \gamma_u \tag{A.1}$$

Similarly the kurtosis of buffeting force is

$$\kappa_L = \frac{\mathbb{E}[L^4]}{\mathbb{E}[L^2]^{4/2}} = \frac{\mathbb{E}[\mathbb{L}(u)^4]}{\mathbb{E}[\mathbb{L}(u)^2]^{4/2}} = \frac{\mathbb{E}[a^4u^4]}{\mathbb{E}[a^2u^2]^{4/2}} = \frac{\mathbb{E}[u^4]}{\mathbb{E}[u^2]^{4/2}} = \kappa_u \tag{A.2}$$

References

[1] Davenport AG. A statistical approach to the treatment of wind loading on tall masts and suspension bridges (Ph.D. Dissertation), United Kingdom: University of Bristol; 1961.
[2] Isyumov N, Alan G. Davenport's mark on wind engineering. J Wind Eng Ind Aerodyn 2012;104:12–24.
[3] Davenport AG. Buffeting of a suspension bridge by storm winds. J Struct Div 1962;88(3):233–70.
[4] Humar J. Dynamics of structures. 3rd ed.. Florida, USA: CRC Press; 2012.
[5] Piccardo G, Solari G. Closed form prediction of 3-D wind-excited response of slender structures. J Wind Eng Ind Aerodyn 1998;74:697–708.
[6] Cui W, Caracoglia L. Examination of experimental variability in HFFB testing of a tall building under multi-directional winds. J Wind Eng Ind Aerodyn 2017;171:34–49.
[7] Cui W, Caracoglia L. Simulation and analysis of intervention costs due to wind-induced damage on tall buildings. Eng Struct 2015;87:183–97.
[8] Gattulli V, Martinelli L, Perotti F, Vestroni F. Dynamics of suspended cables under turbulence loading: reduced models of wind field and mechanical system. J Wind Eng Ind Aerodyn 2007;95(3):183–207.
[9] Caracoglia L, Jones NP. Numerical and experimental study of vibration mitigation for highway light poles. Eng Struct 2007;29(5):821–31.
[10] Scanlan RH, Jones NP. Aeroelastic analysis of cable-stayed bridges. J Struct Eng 1990;116(2):279–97.
[11] Jain A, Jones NP, Scanlan RH. Coupled flutter and buffeting analysis of long-span bridges. J Struct Eng 1996;122(7):716–25.
[12] Katsuchi H, Jones NP, Scanlan RH. Multimode coupled flutter and buffeting analysis of the akashi-kaikyo bridge. J Struct Eng 1999;125(1):60–70.
[13] Domaneschi M, Martinelli L. Refined optimal passive control of buffeting-induced wind loading of a suspension bridge. Wind Struct 2014;18(1):1–20.
[14] Domaneschi M, Martinelli L, Po E. Control of wind buffeting vibrations in a suspension bridge by tmd: Hybridization and robustness issues. Comput Struct 2015;155:3–17.
[15] Scanlan RH. Role of indicial functions in buffeting analysis of bridges. J Struct Eng 1984;110(7):1433–46.
[16] Roger KL, R KL. Airplane math modeling methods for active control design. Tech. rep. AGARD-CP-228, 1977.
[17] Cao S, Tamura Y, Kikuchi N, Saito M, Nakayama I, Matsuzaki Y. Wind characteristics of a strong typhoon. J Wind Eng Ind Aerodyn 2009;97(1):11–21.
[18] Li L, Kareem A, Xiao Y, Song L, Zhou C. A comparative study of field measurements of the turbulence characteristics of typhoon and hurricane winds. J Wind Eng Ind Aerodyn 2015;140:49–66.
[19] Hui Y, Li B, Kawai H, Yang Q. Non-stationary and non-gaussian characteristics of wind speeds. Wind Struct 2017;24(1):59–78.
[20] Gusella V, Materazzi A. Non-gaussian along-wind response analysis in time and frequency domains. Eng Struct 2000;22(1):49–57.
[21] Yang Q, Tian Y. A model of probability density function of non-Gaussian wind pressure with multiple samples. J Wind Eng Ind Aerodyn 2015;140:67–78.
[22] Lutes LD. Cumulants of stochastic response for linear systems. J Eng Mech 1986;112(10):1062–75.
[23] Cui W, Caracoglia L. A fully-coupled generalized model for multi-directional wind loads on tall buildings: A development of the quasi-steady theory. J Fluids Struct 2018;78:52–68.
[24] Cui W, Zhao L, Ge Y. Non-gaussian turbulence induced buffeting responses of long-span bridges. J Bridge Eng 2021;26(8):04021057.
[25] Vanmarcke EH. Properties of spectral moments with applications to random vibration. J Eng Mech Div 1972;98(2):425–46.
[26] Grigoriu M, Ariaratnam ST. Response of linear systems to polynomials of Gaussian processes. J Appl Mech 1988;55(4):905–10.
[27] Grigoriu M. Stochastic calculus: Applications in science and engineering. Boston, MA, USA: Birkhäuser; 2002.
[28] Grigoriu M, Field Jr R. A method for analysis of linear dynamic systems driven by stationary non-gaussian noise with applications to turbulence-induced random vibration. Appl Math Model 2014;38(1):336–54.
[29] Zhao L, Cui W, Ge Y. Measurement, modeling and simulation of wind turbulence in typhoon outer region. J Wind Eng Ind Aerodyn 2019;195:104021.
[30] Yang L, Gurley KR. Efficient stationary multivariate non-Gaussian simulation based on a Hermite pdf model. Probab Eng Mech 2015;42:31–41.
[31] Gioffre M, Gusella V, Grigoriu M. Simulation of non-gaussian field applied to wind pressure fluctuations. Probab Eng Mech 2000;15(4):339–45.
[32] Grigoriu M. Simulation of stationary non-Gaussian translation processes. J Eng Mech 1998;124(2):121–6.
[33] Igusa T, Kiureghian AD, Sackman JL. Modal decomposition method for stationary response of non-classically damped systems. Earthq Eng Struct Dyn 1984;12(1):121–36.
[34] Scanlan R. The action of flexible bridges under wind, i: flutter theory. J Sound Vib 1978;60(2):187–99.
[35] Chen X, Matsumoto M, Kareem A. Time domain flutter and buffeting response analysis of bridges. J Eng Mech 2000;126(1):7–16.
[36] Galleani L, Cohen L. The generalized wiener process for colored noise. IEEE Signal Process Lett 2006;13(10):608–11.
[37] Itô K. Stochastic integral. Proc Imp Acad 1944;20(8):519–24.
[38] Karlin S, Taylor HE. A second course in stochastic processes. Elsevier; 1981.
[39] Seo DW, Caracoglia L. Statistical buffeting response of flexible bridges influenced by errors in aeroelastic loading estimation. J Wind Eng Ind Aerodyn 2012;104:129–40.
[40] Theodorsen T. General theory of aerodynamic instability and the mechanism of flutter. 1935.
[41] Sears WR. Some aspects of non-stationary airfoil theory and its practical application. J Aeronaut Sci 1941;8(3):104–8.
[42] Seo DW, Caracoglia L. Estimating life-cycle monetary losses due to wind hazards: Fragility analysis of long-span bridges. Eng Struct 2013;56:1593–606.
[43] Xu YL, Guo W. Dynamic analysis of coupled road vehicle and cable-stayed bridge systems under turbulent wind. Eng Struct 2003;25(4):473–86.
[44] Isserlis L. On a formula for the product-moment coefficient of any order of a normal frequency distribution in any number of variables. Biometrika 1918;12(1/2):134–9.
[45] Li J, Chen J. Stochastic dynamics of structures. John Wiley & Sons; 2009.
[46] Jones NP, Scanlan RH. Theory and full-bridge modeling of wind response of cable-supported bridges. J Bridge Eng 2001;6(6):365–75.
[47] Gram J. Über die entwickelung reeler funktionen in reihen mittelstder methode der kleinsten quadrate. J Reine Angew Math 1883;94.
[48] Rice SO. Mathematical analysis of random noise. Bell Syst Tech J 1944;23(3):282–332.
[49] Kwon DK, Kareem A. Peak factors for non-gaussian load effects revisited. J Struct Eng 2011;137(12):1611–9.